Supplementary Information for "Geochemistry constrains global hydrology on Early Mars".

Edwin S. Kite[1] and Mohit Melwani Daswani[1,2]

1. University of Chicago, Chicago, IL.

2. Now at: Jet Propulsion Laboratory, Caltech, Pasadena, CA.

1. Detailed description of the CHIM-XPT modeling runs

We used program CHIM-XPT (Reed, 1998) to compute the equilibrium aqueous alteration of Mars basalt and the leaching of ions in a 1-D fluid-centered flow-through pathway through the basalt or olivine-only aquifer (Supplementary Figure 1). The leading fluid parcel reacts and equilibrates with unreacted rock as it moves along the flow path, and is out of contact and out of equilibrium with the preceding rock parcels, so back-reaction of the moving parcel of fluid with the previously altered rock is prevented. Precipitated phases are fractionated from the system at each step along the path (see Bethke, 2007, p. 17; and Reed, 1998, pp. 119–120 for further details). The thermodynamic database, SolthermBRGM[1], contains equilibrium constants for a large number of minerals, chemical species and gases from 0.01 to 600°C and pressures from 1 bar to 5 kbar. SolthermBRGM includes low-temperature species from the BRGM Thermoddem database (Blanc et al., 2012) among others.

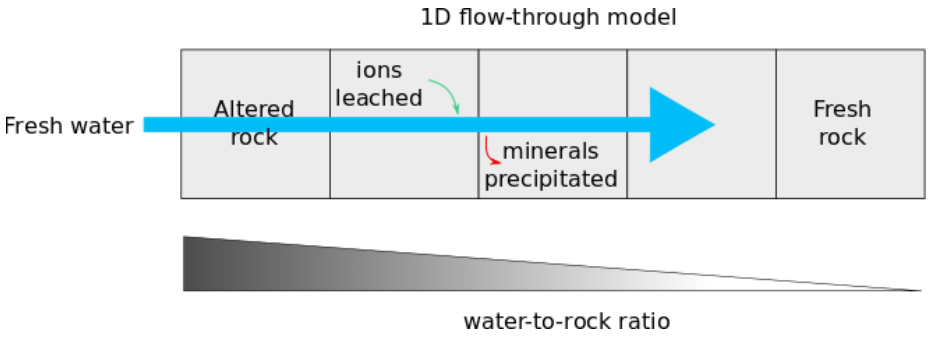

Supplementary Figure 1. Cartoon of the reaction path model carried out with CHIM-XPT. Fresh water equilibrated with the atmosphere equilibrates with sequential parcels of unaltered rock. Along the fluid path, ions are leached from the rock into the fluid, and ions are removed from the fluid into the rock as saturated minerals are precipitated. Water-to-rock ratio decreases from left to right, as the fluid reacts with additional rock.

The reactant rock compositions we used are described in the main text. The composition of the fluids used were initially in equilibrium with the atmosphere pressures shown in SI

[1] Available at https://pages.uoregon.edu/palandri/data/solthermBRGM.xpt.

Table 1, which are based on linear scaling (gas volume/total volume = gas pressure/total pressure) using the current atmosphere's volume mixing ratio (Mahaffy et al., 2013), and ignoring CO because it is minor (<10^{-3} volume ratio) compared to other components.

Supplementary Table 1. Compositions of fresh fluids equilibrated with Mars atmospheres, prior to interaction with the reactant rock. N_2 gas exerts pressure and is soluble in the fluid, but is unreactive in our model and is not taken up by minerals.

Atmospheric pressure (bar)	CO_2 (mol/kg)	HCO_3^- (mol/kg)	CO_3^{2-} (mol/kg)	N_2 (mol/kg)	O_2 (mol/kg)	pH
6×10^{-3}	3.84×10^{-4}	1.04×10^{-5}	2.45×10^{-11}	1.03×10^{-7}	1.63×10^{-8}	4.99
6×10^{-2}	3.84×10^{-3}	3.30×10^{-5}	2.48×10^{-11}	1.03×10^{-6}	1.63×10^{-7}	4.49
2×10^{-1}	1.28×10^{-2}	6.04×10^{-5}	2.51×10^{-11}	3.43×10^{-6}	5.43×10^{-7}	4.23
6×10^{-1}	3.85×10^{-2}	1.05×10^{-4}	2.54×10^{-11}	1.03×10^{-5}	1.63×10^{-6}	3.99
2	1.29×10^{-1}	1.93×10^{-4}	2.59×10^{-11}	3.46×10^{-5}	5.47×10^{-6}	3.73
6	3.91×10^{-1}	3.35×10^{-4}	2.65×10^{-11}	1.05×10^{-4}	1.65×10^{-5}	3.50

We disallowed the formation of specific minerals, aqueous species and gases, such as antigorite and CH_4 (Spreadsheet DISALLOWED_MINERALS.ods) because their formation are kinetically disfavored with low temperature water-rock reactions. The phases allowed to form were vetted to include only phases that would form under the pressure and temperature conditions we have modeled. A number of thermodynamically metastable phases and phases that are not abundant in natural terrestrial basalt-water systems (e.g., thaumasite, $MgHPO_4$, etc.) were allowed in the database because their formation is rapid and kinetically favored. Relevant literature about the natural and synthetic formation conditions of the phases that formed in the models is shown in Supplementary Table 2. Phases like thaumasite that have relatively limited stability fields typically recrystallize into more stable phases in time, especially if burial, heating, and complete dehydration occur. However, in the reaction path models, we quantified the carbon captured at the time that water-rock reaction occurred, and not the fate of carbon after possible recrystallization of metastable phases in time. We think this approach is adequate because the main carbon-bearing phases formed in the models are carbonates, which do not decompose and release CO_2 until reaching ≳450 °C (e.g. Sharp et al., 2003). While some of the phases we allowed to form in the models are unusual in basalt-water systems on Earth, purging the database in order to only include phases commonly associated with terrestrial basalt-water settings risks overlooking potential discoveries on Mars. For example, the Fe-rich amorphous materials analyzed by the *Mars Science Laboratory* throughout Gale Crater (e.g. Bish et al., 2013; Rampe et al., 2017; Vaniman et al., 2014) are clearly one or more metastable phases, that are probably largely chemically unchanged since their formation billions of years ago.

The raw results of the 1-D reaction path models are shown in two supplementary spreadsheet files: one for the basalt aquifer (MARS_BASALT.ods), and another for the olivine-only (MARS_OLIVINE.ods) aquifer.

We show the pH (SI Figure 2), total dissolved aqueous components, and gas fugacities as a function of W/R ratio for each of the modeled scenarios in two animated figures compound for the alteration of the basalt (Supplementary Figure MARS_BASALT.gif) and olivine (Supplementary MARS_OLIVINE.gif) at different CO_2 pressures. By "total dissolved aqueous components", we refer to the total concentration of an element in solution from all the dissolved species bearing that element. For example, the ∑Fe curve is the sum of dissolved iron in the form of Fe^{2+}, $Fe(CO_3)^{2-}$, $Fe(OH)^{+}$, $FeSO_4(aq)$, etc. We also show the secondary minerals precipitated during alteration of the basalt (SI Figures 3 – 8) and olivine, in grams of precipitated mineral per gram of reacted fresh rock (basalt or olivine), per kilogram of water remaining in the system. In the following figures, secondary minerals precipitated in the models are grouped for clarity (e.g., phyllosilicates = kaolinite + smectite + greenalite + …). The individual minerals, their formulae and their groups are described in SI Table 2.

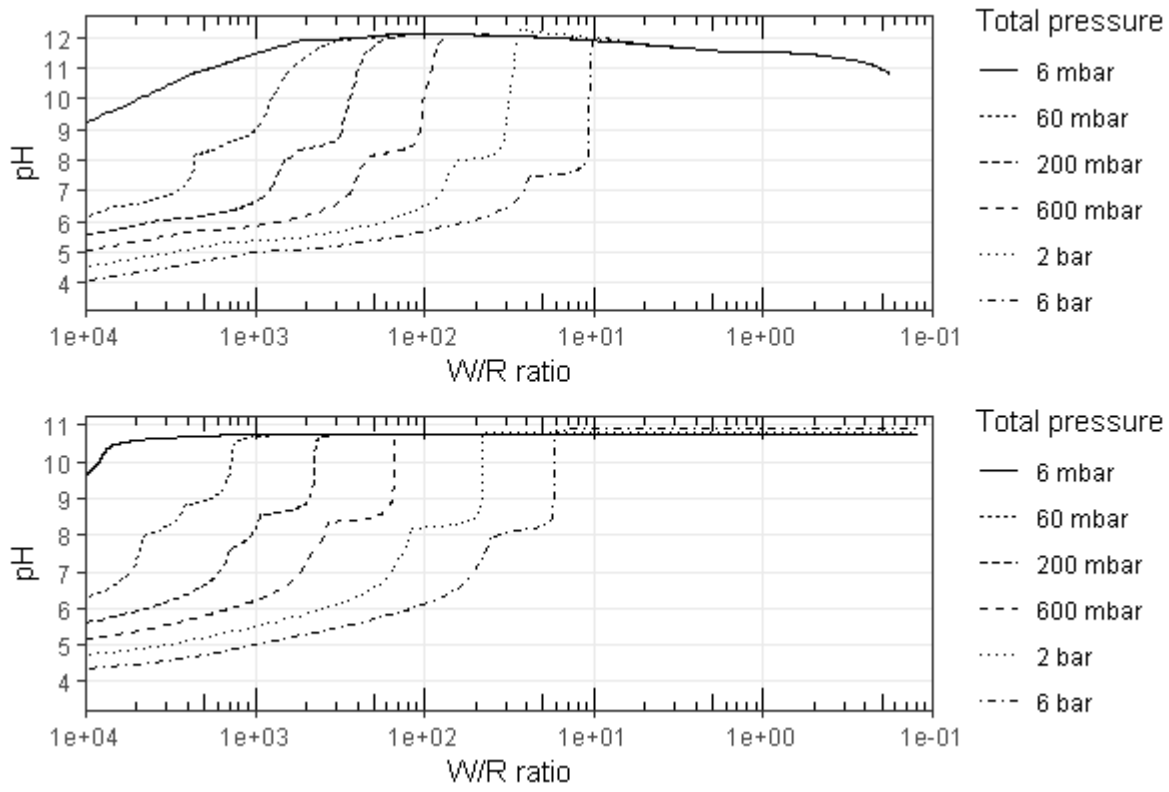

Supplementary Figure 2. Fluid pH for all CHIM-XPT runs at different atmosphere pressures with Mars basalt (top) and Mars olivine (bottom).

At very low W/R ratios (W/R < 1), alteration dry-out tends to occur, resulting in the secondary mineral mass exceeding the amount of fresh rock reacted. The alteration fluid at low W/R already contains a large concentration of dissolved ions, and water tends to be incorporated into minerals (phyllosilicates, zeolites, calcium-silicate-hydrate cements, and hydrous sulfates and phosphates), further increasing the concentration of ions in solution.

Supplementary Table 2. Minerals formed in the basalt and olivine alteration models, their formulae and groups, and relevant literature about their low temperature formation conditions in natural terrestrial and laboratory settings.

Group	Mineral	Formula	Relevant literature about formation conditions
Phosphates	$CaAlH(PO_4)_2{\cdot}6H_2O$	$CaAlH(PO_4)_2{\cdot}6H_2O$	Formed within days in acidic soils (Lehr et al., 1964; Taylor et al., 1964; Taylor and Gurney, 1965, 1964)
	Vivianite	$Fe_3(PO_4)_2{\cdot}8H_2O$	In lacustrine sediments (Rosenqvist, 1970), brackish/marine hypoxic waters (Dijkstra et al., 2016), with siderite in anoxic bogs (Postma, 1980)
	$MgHPO_4$	$MgHPO_4$	Most common phosphate in seawater (Atlas et al., 1976)
	$MnHPO_4$	$MnHPO_4$	Not observed naturally, but thermodynamic data lacking for Mn phosphates (serrabrancite, gatehousite, bermanite, reddingite, hureaulite). $MnHPO_4$ and related Mn phosphates are synthesized in hours to days at low T (Boonchom et al., 2008; Boonchom and Danvirutai, 2008; Evans and Sorensen, 1983)
	$Ca_4H(PO_4)_3{:}3H_2O$	$Ca_4H(PO_4)_3{\cdot}3H_2O$	Octocalcium phosphate, precursor to apatite in (e.g.) coastal and estuarine sediments (Gunnars et al., 2004; Oxmann and Schwendenmann, 2015, 2014)
Phyllosilicates	Kaolinite	$Al_2Si_2O_5(OH)_4$	Common, see also chlorites below. From sedimentation of volcanic ashes in lakes, swamps, lagoons or shallow seas (Meunier, 2005, p. 312)
	Chamosite Clinochlore Al-free chlorite	$Fe_5Al(AlSi_3)O_{10}(OH)_8$ $Mg_5Al(AlSi_3)O_{10}(OH)_8$ $Mg_6Si_4O_{10}(OH)_8$	Chlorites form slowly at low T, but precursor phases form readily as grain coatings and pore infill, and recrystallize (Grigsby, 2001; Wilson and Pittman, 1977); authigenic in soils (Curtis et al., 1985), and in shallow marine environments (Akande and Mücke, 1993). Synthesized at low T in lab (Aja, 2002; Aja and Darby Dyar, 2002)

	Greenalite	$Fe_3Si_2O_5(OH)_4$	Unknown to form authigenically in soils, but gel precipitates at room temperature in anoxic water; structural reorganization and dehydration leads to crystalline greenalite (Tosca et al., 2016).
	Minnesotaite	$Fe_3Si_4O_{10}(OH)_2$	In lateritic weathering, in solid solution with other clay minerals (Harder, 1977). Predicted for Mars (Chevrier et al., 2007; Fairén et al., 2004)
	K-saponite	$K_{0.33}Mg_3Al_{0.33}Si_{3.67}O_{10}(OH)_2$	By reaction of Si+Mg-rich solutions with detrital and basaltic materials in the assemblage of salt lakes, sabkhas and alkaline lakes/swamps (Akbulut and Kadir, 2003; Meunier, 2005, pp. 307–308). Possible composition of the amorphous fraction at Yellowknife Bay on Mars (Bristow et al., 2015)
	Na-saponite	$Na_{0.33}Mg_3Al_{0.33}Si_{3.67}O_{10}(OH)_2$	
	Sepiolite	$Mg_4Si_6O_{15}(OH)_2{\cdot}6H_2O$	Precipitated in alkaline lakes/swamps (Akbulut and Kadir, 2003), and closed basin playa evaporites (Singer et al., 1998). Precipitated from seawater-like composition in lab (Baldermann et al., 2018)
	Smectite(MX_{80}:$5.189H_2O$)	$Na_{0.409}K_{0.024}Ca_{0.009}(Si_{3.738}Al_{0.262})(Al_{1.598}Mg_{0.214}Fe_{0.208})O_{10}(OH)_2{\cdot}5.189H_2O$	From sedimentation of volcanic ashes in lakes, swamps, lagoons or shallow seas (Meunier, 2005, p. 312), in soils derived from basalt weathering (Curtin and Smillie, 1981). Synthesized in lab (Harder, 1972). Detected from orbit and in situ on Mars (Bishop et al., 2018; Clark et al., 2007)
	Mg,Na-montmorillonite	$Na_{0.34}Mg_{0.34}Al_{1.66}Si_4O_{10}(OH)_2$	
	HcK-montmorillonite	$K_{0.6}Mg_{0.6}Al_{1.4}Si_4O_{10}(OH)_2$	
	HcNa-montmorillonite	$Na_{0.6}Mg_{0.6}Al_{1.4}Si_4O_{10}(OH)_2$	
Sulfides	Pyrite	FeS_2	Most thermodynamically stable Fe-disulfide in sediments, formed by precursor amorphous FeS converting to FeS_2 (Schoonen, 2004). Precipitated in brackish water sediments (Postma, 1982)
Carbonates	Calcite	$CaCO_3$	Carbonate precipitation common at low temperature. Siderite precipitation may be slow, but precursor phases precipitate rapidly, and then recrystallize (Jiang and Tosca, 2019; Jimenez-Lopez
	Siderite	$FeCO_3$	
	Ankerite	$CaFe(CO_3)_2$	

			and Romanek, 2004; Romanek et al., 2009)
Zeolites	Chabazite	$Ca(Al_2Si_4)O_{12}\cdot 6H_2O$	Low T zeolites occurring as alteration products of volcanic and feldspathic rocks often volcanoclastics flushed by saline groundwater (Chipera and Apps, 2001; Hay and Sheppard, 2001; Ming and Boettinger, 2001; Warren, 2015, pp. 1292–1300)
	Ca-phillipsite	$Ca_{0.5}AlSi_3O_8\cdot 3H_2O$	
	K-phillipsite	$KAlSi_3O_8\cdot 3H_2O$	
	Na-phillipsite	$NaAlSi_3O_8\cdot 3H_2O$	
	Ca-clinoptilolite	$Ca_{0.55}(Si_{4.9}Al_{1.1})O_{12}\cdot 3.9H_2O$	
Calcium-silicate-hydrates	Thaumasite	$CaSiO_3CaSO_4CaCO_3\cdot 15H_2O$	Low T seawater reaction with basalts and tuffs (Grubessi et al., 1986; Karpoff et al., 1992; Noack, 1983), and alteration of volcanic rocks in Antarctic Dry Valleys (Keys and Williams, 1981). Precipitates rapidly in lab, and destabilizes at >30 °C (Matschei et al., 2007; Pipilikaki et al., 2008; Schmidt et al., 2008)
	CSH(1.2)	$Ca_{1.2}SiO_{3.2}\cdot 2.06H_2O$	Tobermorite-like cement phases formed by weathering of metamorphosed carbonate + clay mineral-rich rocks (Gross, 2016, 1977). Precipitates within days in lab (Dilnesa, 2012; Gross, 1981; Schmidt et al., 2008)
Sulfates	Gypsum	$CaSO_4\cdot 2H_2O$	Common, especially from saturation and evaporation of saline fluid (e.g. Corselli and Aghib, 1987), but also alteration of basalt (e.g. McCanta et al., 2014)
Silica	Amorphous silica	SiO_2	Common. For Mars see e.g., discussion by McAdam et al. (McAdam et al., 2008).
Iron oxides	Goethite	FeOOH	Common
	Magnetite	Fe_3O_4	From dissolution-precipitation of Fe-rich material and in soils (Maher and Taylor, 1988; Spiroff, 1938; Taylor et al., 1986). Precipitation from solution in lab (Hansel et al., 2005; Vayssières et al., 1998).

1.1. Basalt alteration

Basalt alteration with CO_2-charged water causes the formation of carbonates and the drawdown of carbon under all initial pCO_2 conditions. Carbon drawdown begins with siderite formation and precipitation at high W/R ratios (SI Figure 3). H^+ produced from the dissociation of carbonic acid:

$$H_2CO_3 + H_2O \rightarrow HCO_3^- + H_3O^+ \qquad (1)$$

is consumed by the dissolution of olivine and pyroxene as the fluid encounters fresh rock:

$$MgFeSiO_4 \text{ (olivine)} + 2H_3O^+ \rightarrow Mg^{2+} + Fe^{2+} H_4SiO_4 + 2OH^- \quad (2)$$

$$Mg_{0.5}Fe_{0.5}SiO_3 \text{ (pyroxene)} + H_3O^+ \rightarrow Mg_{0.5}^{2+} + Fe_{0.5}^{2+} + H_2SiO_3 + OH^- \qquad (3)$$

These reactions are strongly favored while the CO_2-charged fluid reacts with fresh rock but are limited by the amount of initial CO_2. When almost all carbonic acid is consumed, pH increases sharply (SI Figure 2a) as OH^- produced from the breakdown of olivine and pyroxene (Reactions 2 and 3) is unbuffered by further dissociation of carbonic acid (Reaction 1). While carbonate and bicarbonate anions are supplied by the dissociation of carbonic acid, carbonates precipitate (SI Figures 3 – 8) as siderite, ankerite and calcite.

At lower W/R ratios, when most carbonate is removed along the fluid path, the fluid becomes reducing, when the predominant phyllosilicates minnesotaite ($Fe_3Si_4O_{10}(OH)_2$) and $Na_{0.409}K_{0.024}Ca_{0.009}(Si_{3.738}Al_{0.262})(Al_{1.598}Mg_{0.214}Fe_{0.208})O_{10}(OH)_2 \cdot 5.189H_2O$ (a smectite of the montmorillonite group) stop precipitating in favor of greenalite ($Fe_3Si_2O_5(OH)_4$), which removes a larger amount of oxidants (namely OH^-) from solution per gram precipitated. Na-phillipsite ($NaAlSi_3O_8 \cdot 3H_2O$), and calcium-silicate-hydrate 1.2 ($Ca_{1.2}SiO_{3.2} \cdot 2.06H_2O$) provide the main sinks for Na, Al and Ca, while K is only weakly taken up by K-saponite ($K_{0.33}Mg_3Al_{0.33}Si_{3.67}O_{10}(OH)_2$), which allows the dissolved K concentration to increase at lower W/R ratios. Any remaining dissolved carbon is precipitated and removed as thaumasite ($Ca_3Si(OH)_6(CO_3)(SO_4) \cdot 12H_2O$). However, note that thaumasite only forms after most initial CO_2 is taken up by carbonates precipitated out along the reaction path (Supplementary Figures 3 – 8); carbonates require higher pCO_2 than thaumasite to form, and thaumasite only forms after pCO_2 has dropped below this level. Thaumasite is not a major CO_2 sink: each gram of siderite ($FeCO_3$) contains ~0.38 g of CO_2 whereas each gram of thaumasite ($CaSiO_3CaSO_4CaCO_3 \cdot 15H_2O$) contains ~0.07g of CO_2. In all the reaction path models, by far the most dramatic drop in CO_2 fugacity and dissolved carbon coincides with carbonate precipitation (Supplementary Figures 3 – 8).

At W/R < 10, all basalt alteration scenarios converge, yielding nearly equal pH levels, concentrations of aqueous components and precipitated minerals. Small amounts of gypsum ($CaSO_4 \cdot 2H_2O$) precipitate at W/R < 2.

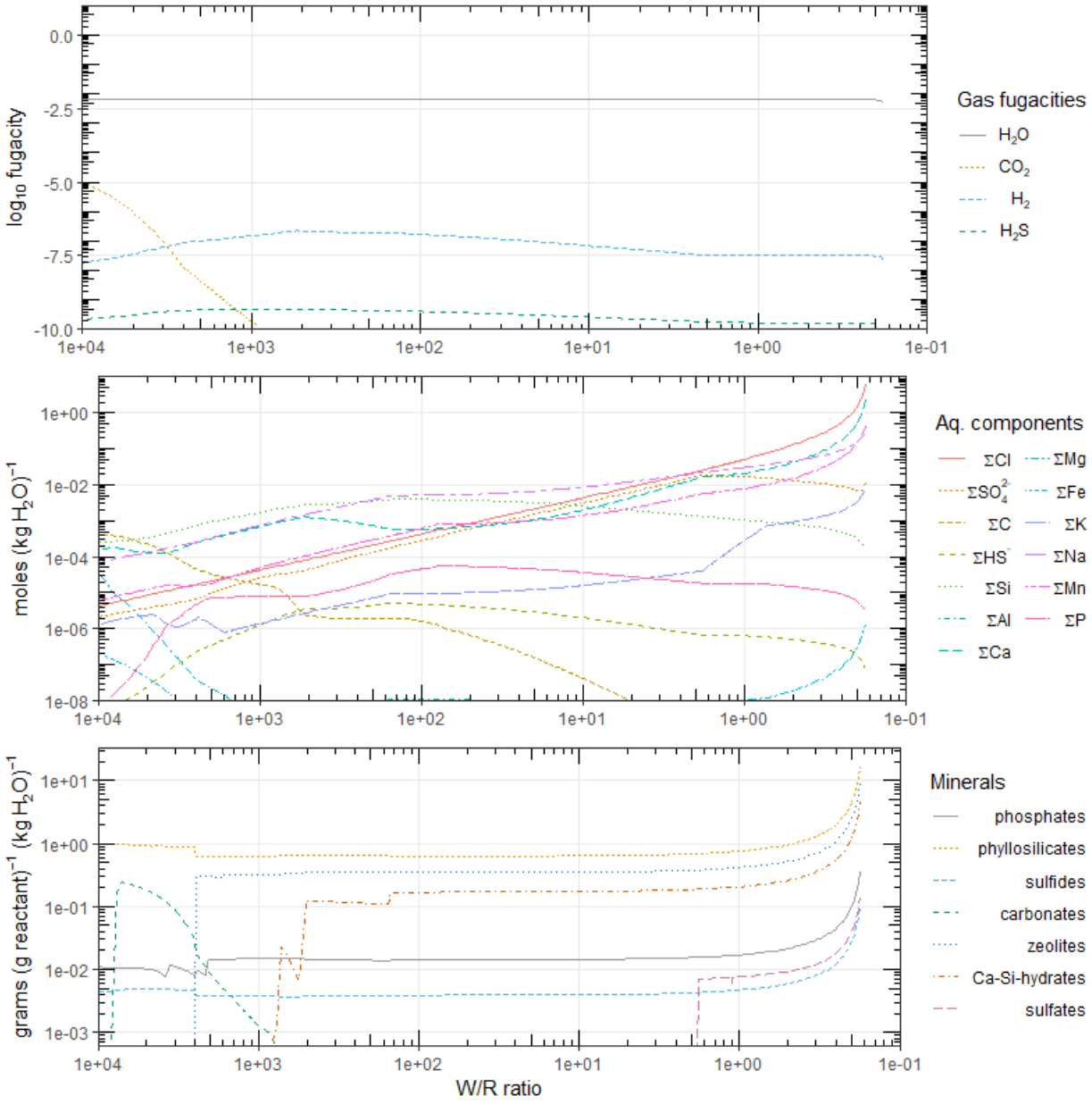

Supplementary Figure 3. Alteration of Mars basalt with fluid initially equilibrated with a 6 mbar atmosphere. Top: gas fugacities; middle: aqueous components in the fluid; bottom: secondary minerals precipitated along the alteration pathway.

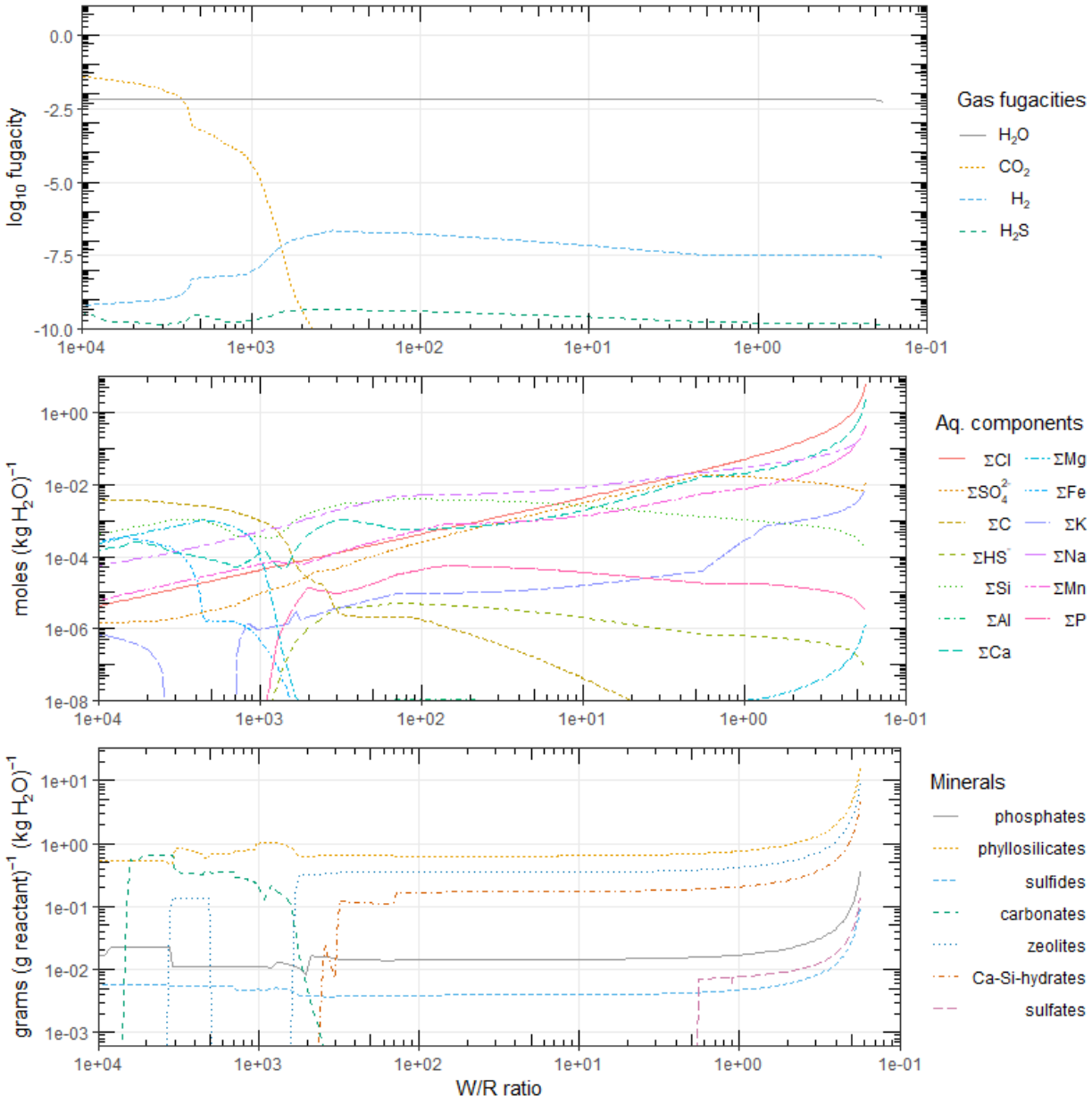

Supplementary Figure 4. Alteration of Mars basalt with fluid initially equilibrated with a 60 mbar atmosphere. Top: gas fugacities; middle: aqueous components in the fluid; bottom: secondary minerals precipitated along the alteration pathway.

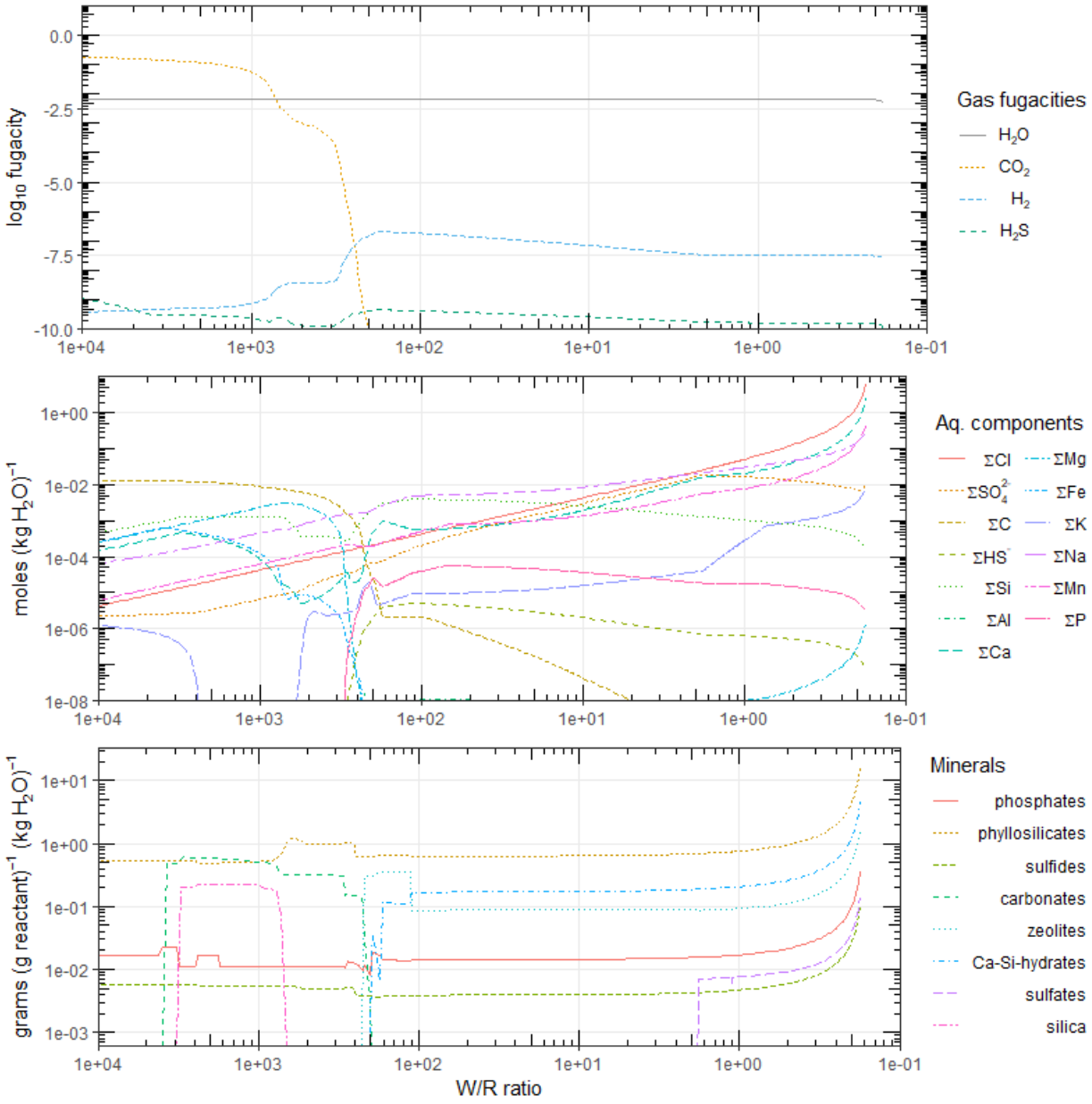

Supplementary Figure 5. Alteration of Mars basalt with fluid initially equilibrated with a 200 mbar atmosphere. Top: gas fugacities; middle: aqueous components in the fluid; bottom: secondary minerals precipitated along the fluid pathway.

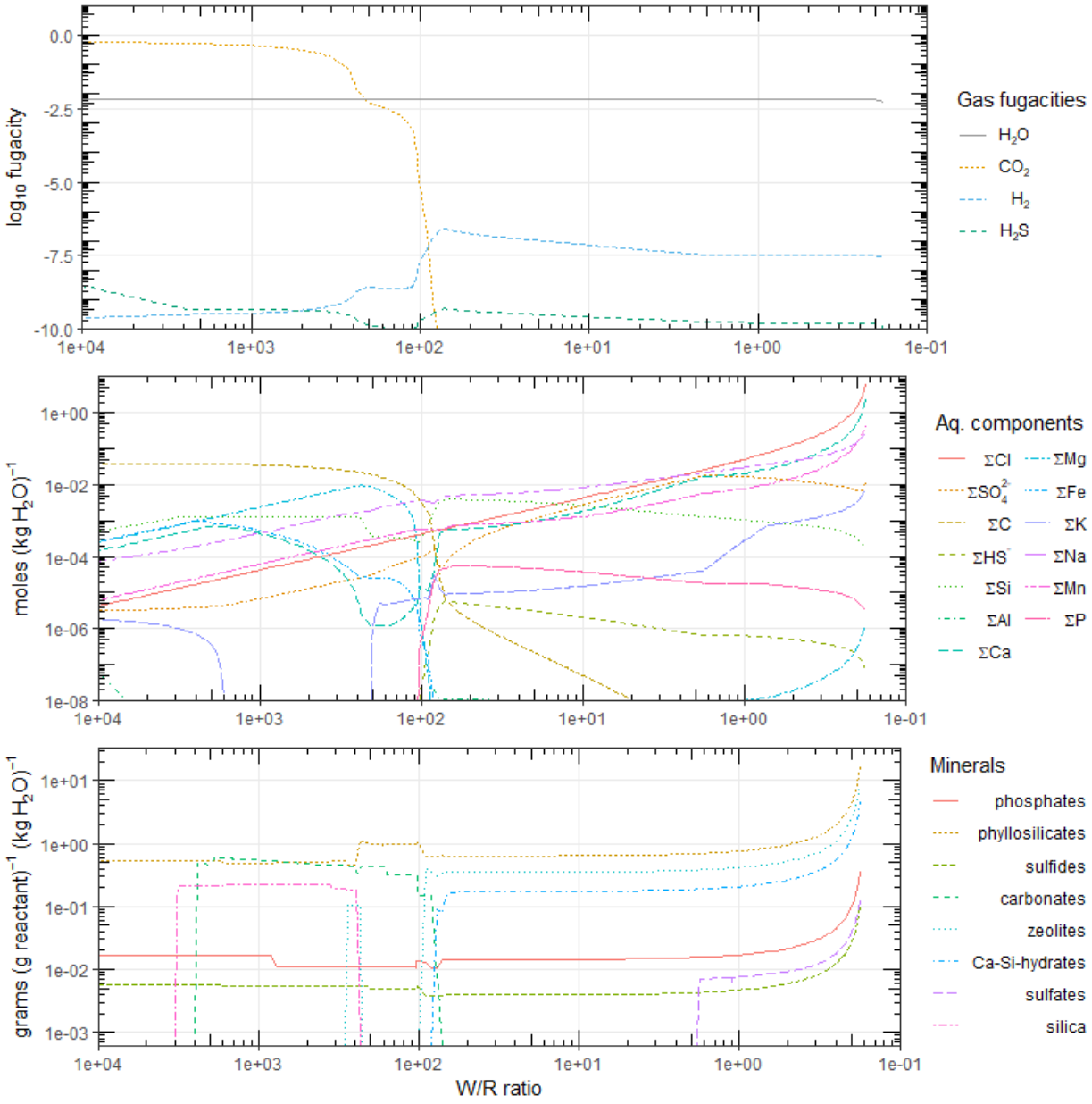

Supplementary Figure 6. Alteration of Mars basalt with fluid initially equilibrated with a 600 mbar atmosphere. Top: gas fugacities; middle: aqueous components in the fluid; bottom: secondary minerals precipitated along the fluid pathway.

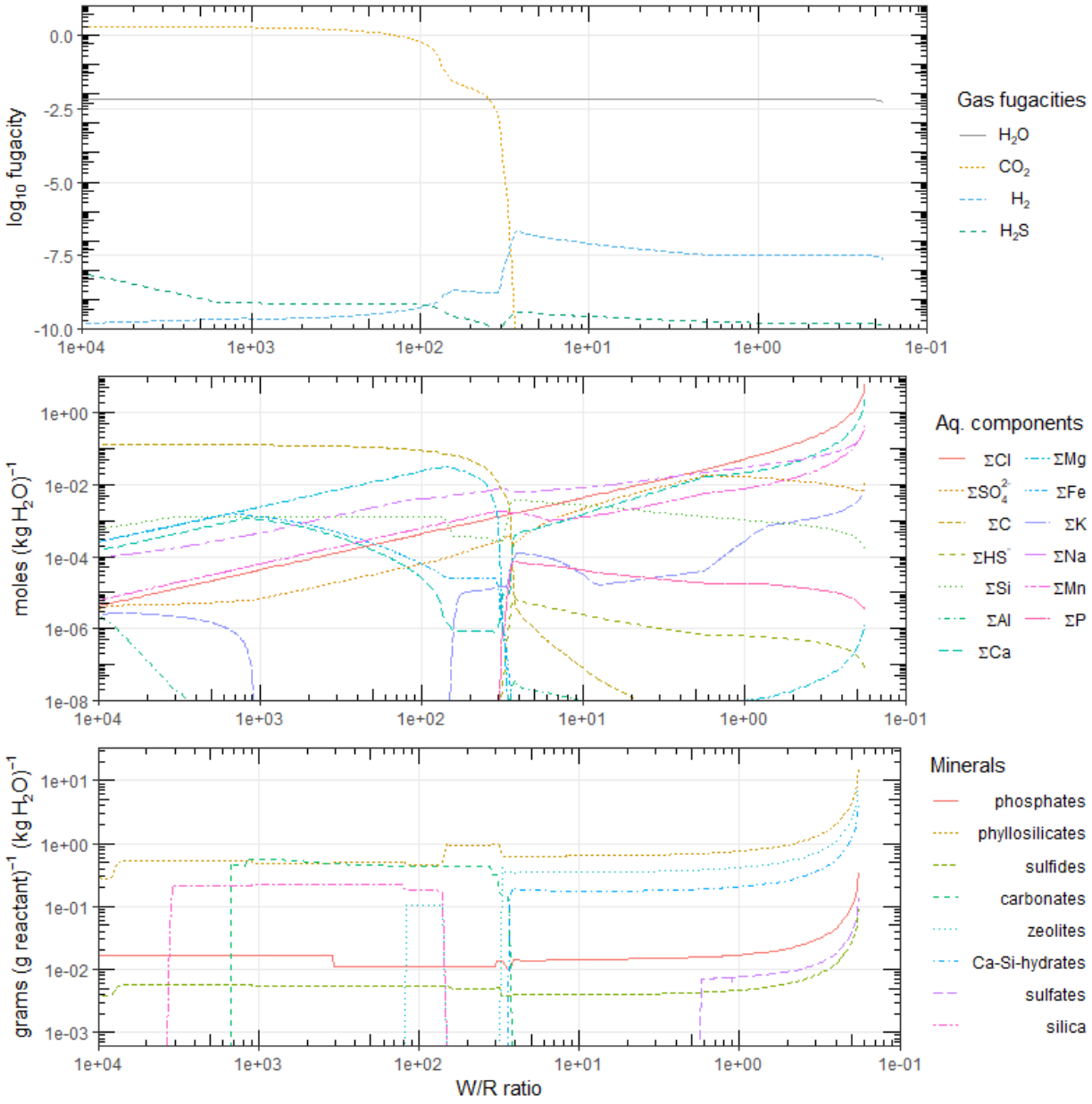

Supplementary Figure 7. Alteration of Mars basalt with fluid initially equilibrated with a 2 bar atmosphere. Top: gas fugacities; middle: aqueous components in the fluid; bottom: secondary minerals precipitated along the fluid pathway.

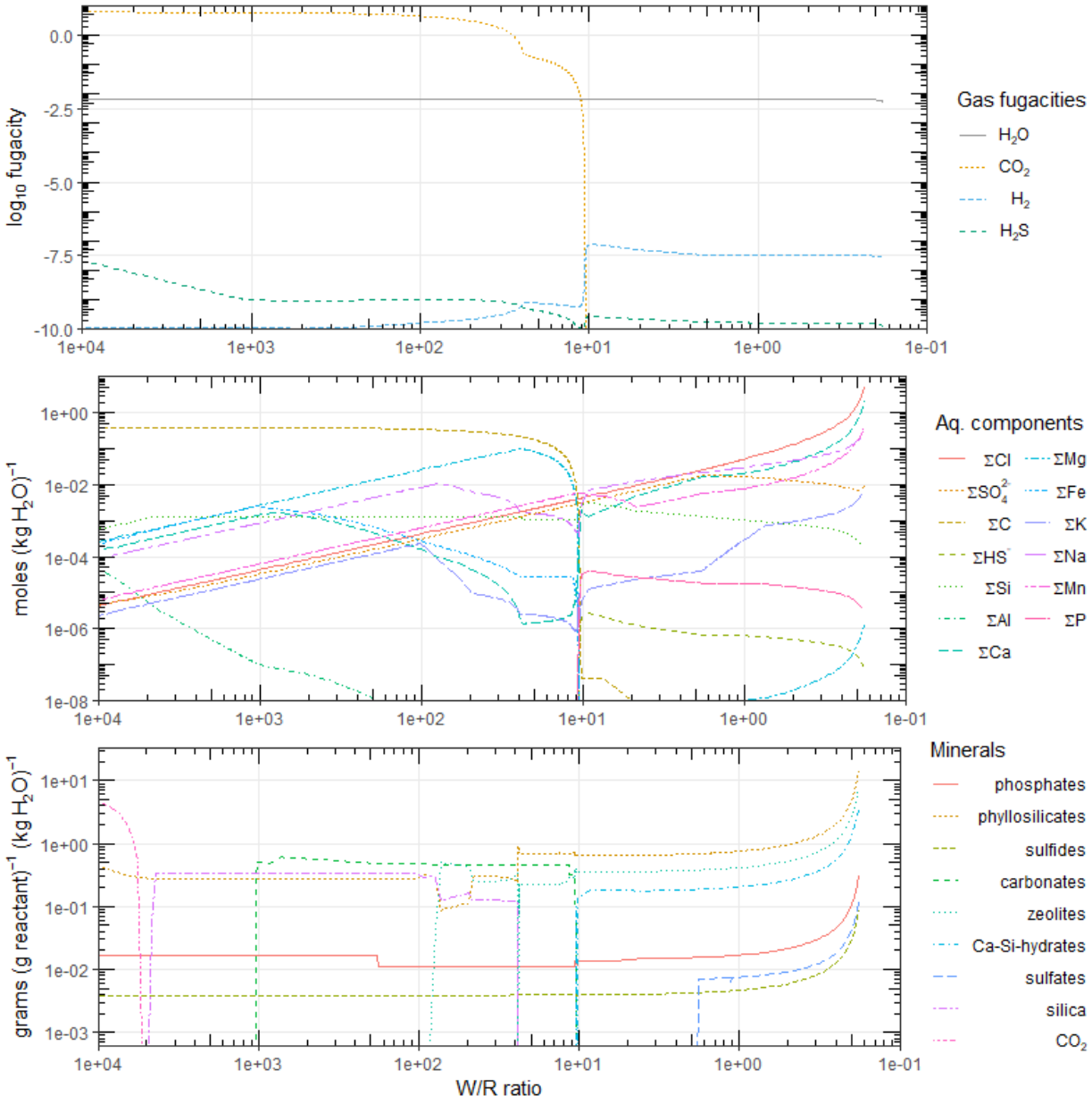

Supplementary Figure 8. Alteration of Mars basalt with fluid initially equilibrated with a 6 bar atmosphere. Top: gas fugacities; middle: aqueous components in the fluid; bottom: secondary minerals precipitated along the fluid pathway.

1.2. Olivine alteration

Reaction of olivine with the CO_2-bearing fluid generally follows a similar pattern to basalt alteration (SI § 1.1), in that Reaction 2 consumes acidity to produce aqueous silica and cations for carbonate minerals. Additionally, FeO dissolved from olivine drives the increase in fluid pH in a series of reactions that culminate in the production of H_2 and magnetite:

$$FeO \text{ (from olivine)} + H_2O \rightarrow Fe^{2+} + 2OH^- \quad (4)$$

$$3Fe_2SiO_4 + 2H_2O = 3SiO_2(aq) + 2Fe_3O_4 + 2H_2(aq) \quad (5)$$

Since the reactant olivine composition lacks calcium, the carbonates precipitated were siderite and hydromagnesite ($Mg_5(OH)_2(CO_3)_4 \cdot 4H_2O$, only at initial pCO_2 = 6 bar and 40 > W/R > 30). However, after most carbonate formation has occurred and pH is buffered to high levels (pH ≈ 10.8), total dissolved carbon ($\sum C$) plateaus at ~5×10^{-5} mol/kg water for all initial pCO_2 conditions tested; precipitation of thaumasite does not occur since it requires sulfate and calcium.

Finally, since the reactant lacks aluminum, all silica sinks from olivine alteration (amorphous silica, sepiolite, Al-free chlorite and greenalite) lack aluminum.

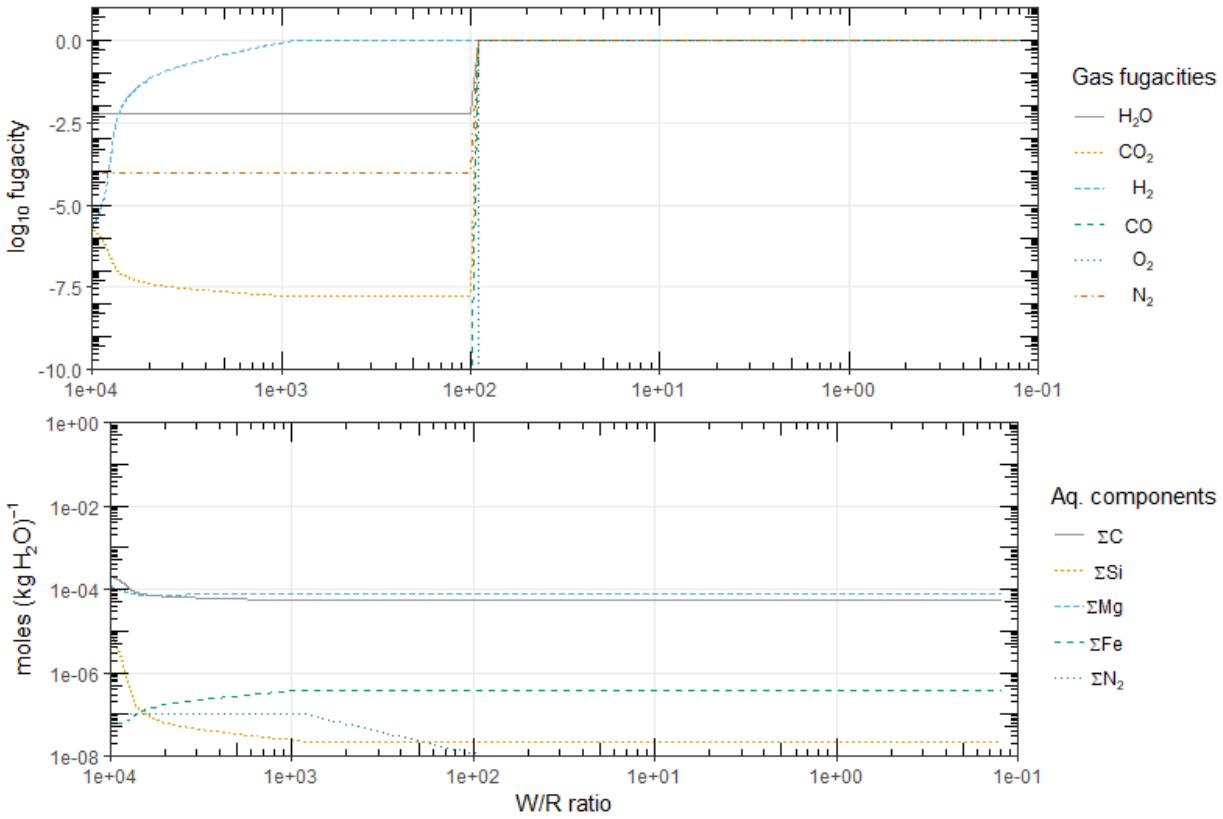

Supplementary Figure 9. Alteration of Mars olivine with fluid initially equilibrated with a 6 mbar atmosphere. Top: gas fugacities; bottom: aqueous components in the fluid.

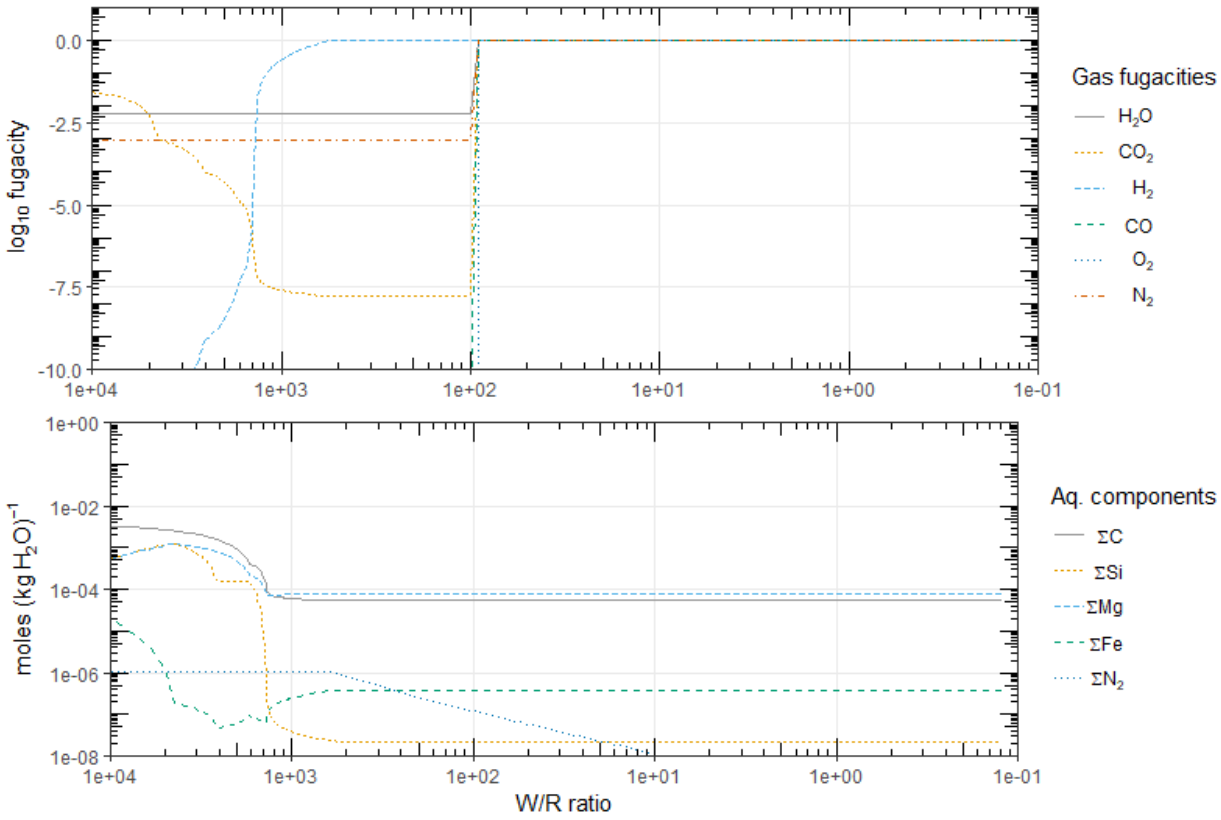

Supplementary Figure 10. Alteration of Mars olivine with fluid initially equilibrated with a 60 mbar atmosphere. Top: gas fugacities; bottom: aqueous components in the fluid.

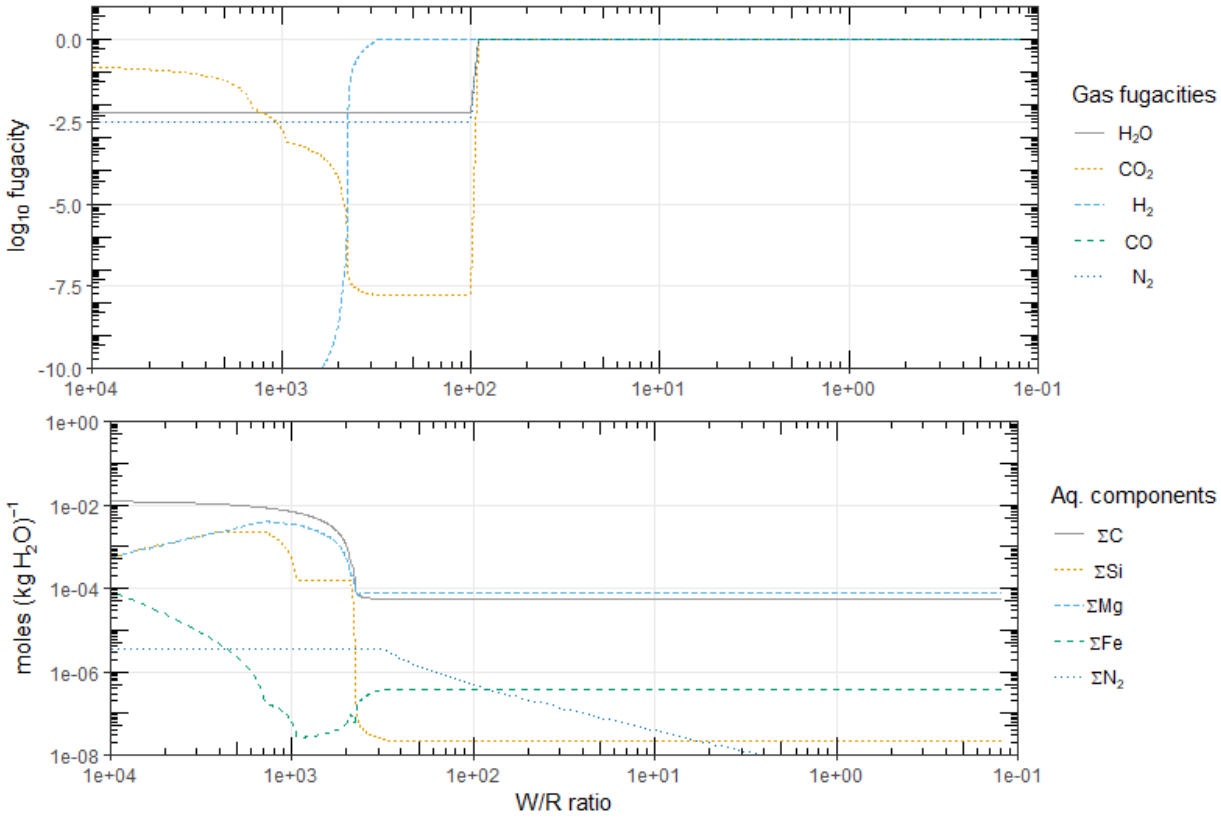

Supplementary Figure 11. Alteration of Mars olivine with fluid initially equilibrated with a 200 mbar atmosphere. Top: gas fugacities; bottom: aqueous components in the fluid.

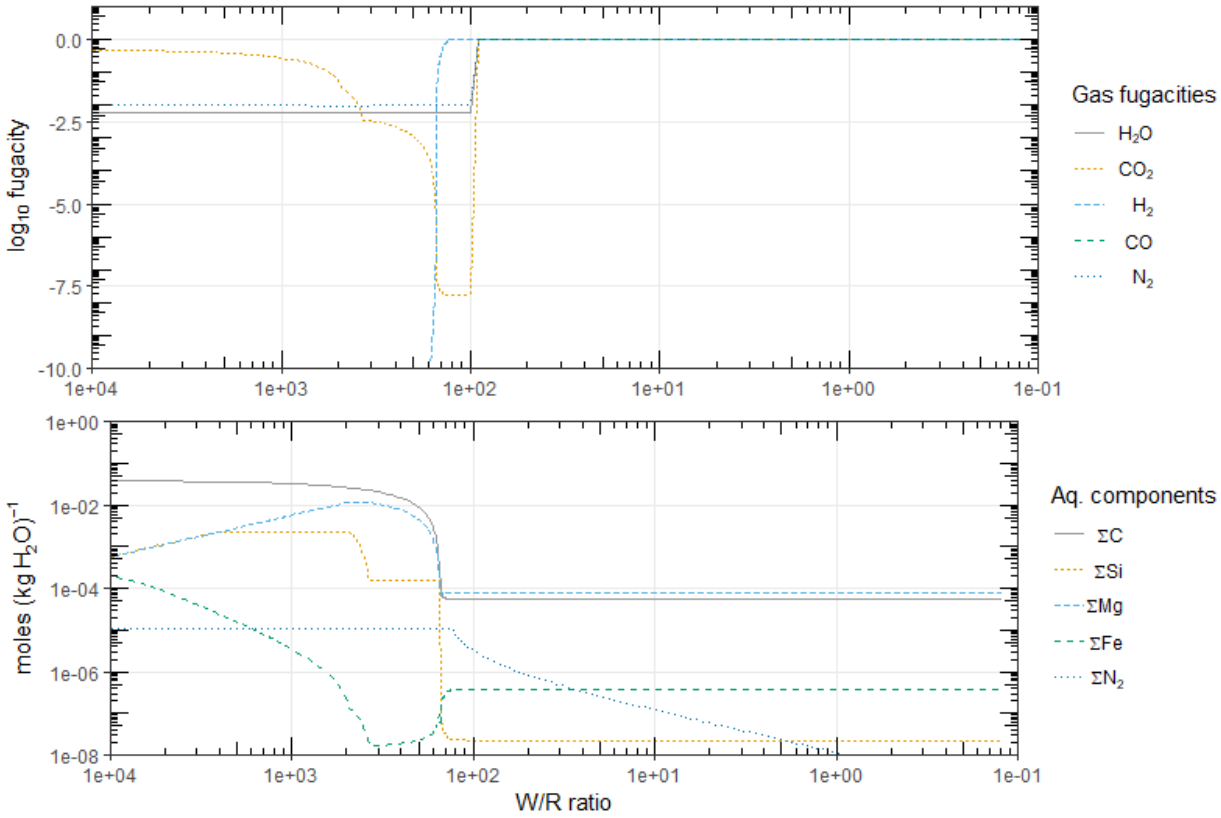

Supplementary Figure 12. Alteration of Mars olivine with fluid initially equilibrated with a 600 mbar atmosphere. Top: gas fugacities; bottom: aqueous components in the fluid.

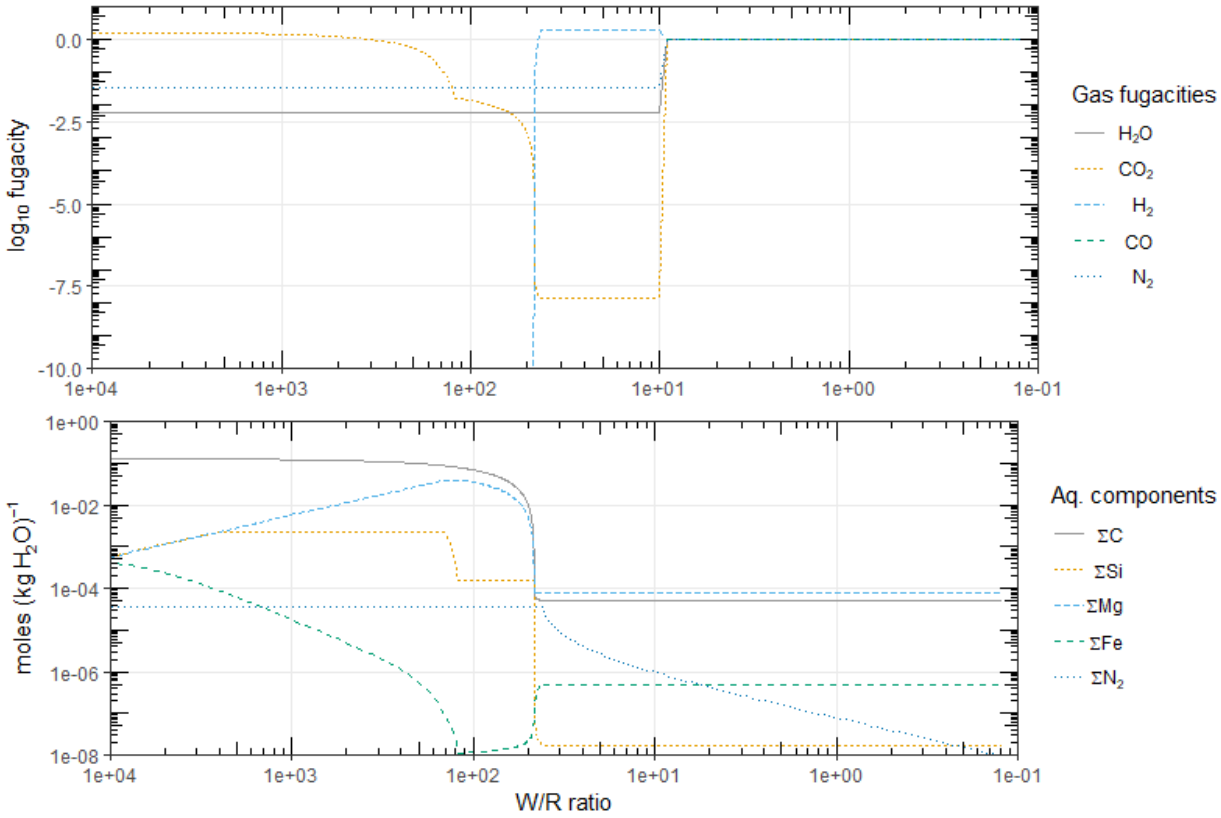

Supplementary Figure 13. Alteration of Mars olivine with fluid initially equilibrated with a 2 bar atmosphere. Top: gas fugacities; bottom: aqueous components in the fluid.

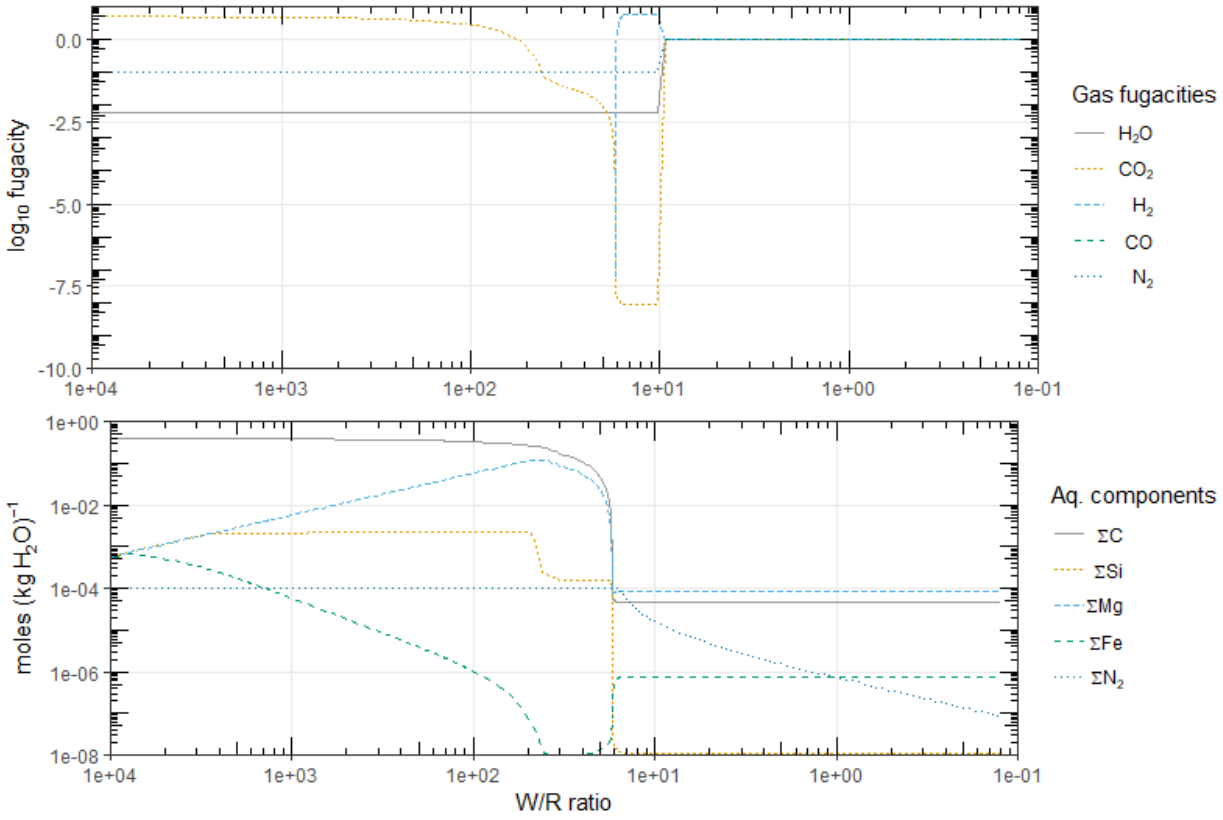

Supplementary Figure 14. Alteration of Mars olivine with fluid initially equilibrated with a 6 bar atmosphere. Top: gas fugacities; bottom: aqueous components in the fluid.

References:

Aja, S.U., 2002. The stability of Fe-Mg chlorites in hydrothermal solutions: II. Thermodynamic properties. Clays and Clay Minerals 50, 591–600.

Aja, S.U., Darby Dyar, M., 2002. The stability of Fe–Mg chlorites in hydrothermal solutions—I. Results of experimental investigations. Applied Geochemistry 17, 1219–1239. https://doi.org/10.1016/S0883-2927(01)00131-7

Akande, S.O., Mücke, A., 1993. Depositional environment and diagenesis of carbonates at the Mamu/Nkporo formation, anambra basin, Southern Nigeria. Journal of African Earth Sciences (and the Middle East) 17, 445–456. https://doi.org/10.1016/0899-5362(93)90003-9

Akbulut, A., Kadir, S., 2003. The Geology and Origin of Sepiolite, Palygorskite and Saponite in Neogene Lacustrine Sediments of the Serinhisar-Acipayam Basin, Denizli, SW Turkey. Clays and Clay Minerals 51, 279–292. https://doi.org/10.1346/CCMN.2003.0510304

Atlas, E., Culberson, C., Pytkowicz, R.M., 1976. Phosphate association with Na+, Ca2+ and Mg2+ in seawater. Marine Chemistry 4, 243–254. https://doi.org/10.1016/0304-4203(76)90011-6

Baldermann, A., Mavromatis, V., Frick, P.M., Dietzel, M., 2018. Effect of aqueous Si/Mg ratio and pH on the nucleation and growth of sepiolite at 25 °C. Geochimica et Cosmochimica Acta 227, 211–226. https://doi.org/10.1016/j.gca.2018.02.027

Bethke, C.M., 2007. Geochemical and biogeochemical reaction modeling. Cambridge University Press.

Bish, D.L., Blake, D.F., Vaniman, D.T., Chipera, S.J., Morris, R.V., Ming, D.W., Treiman, A.H., Sarrazin, P., Morrison, S.M., Downs, R.T., Achilles, C.N., Yen, A.S., Bristow, T.F., Crisp, J.A., Morookian, J.M., Farmer, J.D., Rampe, E.B., Stolper, E.M., Spanovich, N., MSL Science Team, 2013. X-ray Diffraction Results from Mars Science Laboratory: Mineralogy of Rocknest at Gale Crater. Science 341. https://doi.org/10.1126/science.1238932

Bishop, J.L., Fairén, A.G., Michalski, J.R., Gago-Duport, L., Baker, L.L., Velbel, M.A., Gross, C., Rampe, E.B., 2018. Surface clay formation during short-term warmer and wetter conditions on a largely cold ancient Mars. Nature Astronomy 2, 206–213. https://doi.org/10.1038/s41550-017-0377-9

Blanc, Ph., Lassin, A., Piantone, P., Azaroual, M., Jacquemet, N., Fabbri, A., Gaucher, E.C., 2012. Thermoddem: A geochemical database focused on low temperature water/rock interactions and waste materials. Appl. Geochem. 27, 2107–2116. https://doi.org/10.1016/j.apgeochem.2012.06.002

Boonchom, B., Danvirutai, C., 2008. A simple synthesis and thermal decomposition kinetics of MnHPO4· H2O rod-like microparticles obtained by spontaneous precipitation route. Journal of optoelectronics and advanced materials 10, 492–499.

Boonchom, B., Youngme, S., Maensiri, S., Danvirutai, C., 2008. Nanocrystalline serrabrancaite (MnPO4·H2O) prepared by a simple precipitation route at low temperature. Journal of Alloys and Compounds 454, 78–82. https://doi.org/10.1016/j.jallcom.2006.12.064

Bristow, T.F., Bish, D.L., Vaniman, D.T., Morris, R.V., Blake, D.F., Grotzinger, J.P., Rampe, E.B., Crisp, J.A., Achilles, C.N., Ming, D.W., Ehlmann, B.L., King, P.L., Bridges, J.C., Eigenbrode, J.L., Sumner, D.Y., Chipera, S.J., Moorokian, J.M., Treiman, A.H., Morrison, S.M., Downs, R.T., Farmer, J.D., Marais, D.D., Sarrazin, P., Floyd, M.M., Mischna, M.A., McAdam, A.C., 2015. The origin and implications of clay minerals from Yellowknife Bay, Gale crater, Mars†. American Mineralogist 100, 824–836. https://doi.org/10.2138/am-2015-5077CCBYNCND

Chevrier, V., Poulet, F., Bibring, J.-P., 2007. Early geochemical environment of Mars as determined from thermodynamics of phyllosilicates. Nature 448, 60–63. https://doi.org/10.1038/nature05961

Chipera, S.J., Apps, J.A., 2001. Geochemical Stability of Natural Zeolites. Reviews in Mineralogy and Geochemistry 45, 117–161. https://doi.org/10.2138/rmg.2001.45.3

Clark, B.C., Arvidson, R.E., Gellert, R., Morris, R.V., Ming, D.W., Richter, L., Ruff, S.W., Michalski, J.R., Farrand, W.H., Yen, A., Herkenhoff, K.E., Li, R., Squyres, S.W., Schröder, C., Klingelhöfer, G., Bell, J.F., 2007. Evidence for montmorillonite or its compositional equivalent in Columbia Hills, Mars. Journal of Geophysical Research: Planets 112, E06S01. https://doi.org/10.1029/2006JE002756

Corselli, C., Aghib, F.S., 1987. Brine formation and gypsum precipitation in the Bannock Basin, Eastern Mediterranean. Marine Geology 75, 185–199. https://doi.org/10.1016/0025-3227(87)90103-4

Curtin, D., Smillie, G.W., 1981. Composition and Origin of Smectite in Soils Derived from Basalt in Northern Ireland. Clays and Clay Minerals 29, 277–284. https://doi.org/10.1346/CCMN.1981.0290405

Curtis, C.D., Murchison, D.G., Berner, R.A., Shaw, H., Sarnthein, M., Durand, B., Eglinton, G., Mackenzie, A.S., Surdam, R.C., 1985. Clay Mineral Precipitation and Transformation during Burial Diagenesis [and Discussion]. Philosophical Transactions of the Royal Society of London. Series A, Mathematical and Physical Sciences 315, 91–105. https://doi.org/10.1098/rsta.1985.0031

Dijkstra, N., Slomp, C.P., Behrends, T., 2016. Vivianite is a key sink for phosphorus in sediments of the Landsort Deep, an intermittently anoxic deep basin in the Baltic Sea. Chemical Geology 438, 58–72. https://doi.org/10.1016/j.chemgeo.2016.05.025

Dilnesa, B.Z., 2012. Fe-containing Hydrates and their Fate during Cement Hydration : Thermodynamic Data and Experimental Study. EPFL, Lausanne.

Evans, A., Sorensen, R.C., 1983. Determination of the kinnetic order and heaction parameters for Cd3(PO4)2 and MnHPO4. Communications in Soil Science and Plant Analysis 14, 773–783. https://doi.org/10.1080/00103628309367407

Fairén, A.G., Fernández-Remolar, D., Dohm, J.M., Baker, V.R., Amils, R., 2004. Inhibition of carbonate synthesis in acidic oceans on early Mars. Nature 431, 423–426. https://doi.org/10.1038/nature02911

Grigsby, J.D., 2001. Origin and Growth Mechanism of Authigenic Chlorite in Sandstones of the Lower Vicksburg Formation, South Texas. Journal of Sedimentary Research 71, 27–36. https://doi.org/10.1306/060100710027

Gross, S., 2016. Petrographic atlas of the Hatrurim Formation (No. GSI/05/2016). Geological Survey of Israel, Jerusalem.

Gross, S., 1981. Simulation of natural weathering processes in the Hatrurim Formation. Current research - Geological Survey of Israel 1981, 6–8.

Gross, S., 1977. The mineralogy of Hatrurim Formation, Israel. Geol. Surv. Israel, Bull. 70, 1–80.

Grubessi, O., Mottana, A., Paris, E., 1986. Thaumasite from the Tschwinning mine, South Africa. Tschermaks mineralogische und petrographische Mitteilungen 35, 149–156. https://doi.org/10.1007/BF01082082

Gunnars, A., Blomqvist, S., Martinsson, C., 2004. Inorganic formation of apatite in brackish seawater from the Baltic Sea: an experimental approach. Marine Chemistry 91, 15–26. https://doi.org/10.1016/j.marchem.2004.01.008

Hansel, C.M., Benner, S.G., Fendorf, S., 2005. Competing Fe(II)-Induced Mineralization Pathways of Ferrihydrite. Environ. Sci. Technol. 39, 7147–7153. https://doi.org/10.1021/es050666z

Harder, H., 1977. Clay mineral formation under lateritic weathering conditions. Clay Minerals 12, 281–288. https://doi.org/10.1180/claymin.1977.012.4.01

Harder, H., 1972. The role of magnesium in the formation of smectite minerals. Chemical Geology 10, 31–39. https://doi.org/10.1016/0009-2541(72)90075-7

Hay, R.L., Sheppard, R.A., 2001. Occurrence of Zeolites in Sedimentary Rocks: An Overview. Reviews in Mineralogy and Geochemistry 45, 217–234. https://doi.org/10.2138/rmg.2001.45.6

Jiang, C.Z., Tosca, N.J., 2019. Fe(II)-carbonate precipitation kinetics and the chemistry of anoxic ferruginous seawater. Earth and Planetary Science Letters 506, 231–242. https://doi.org/10.1016/j.epsl.2018.11.010

Jimenez-Lopez, C., Romanek, C.S., 2004. Precipitation kinetics and carbon isotope partitioning of inorganic siderite at 25°C and 1 atm. Geochimica et Cosmochimica Acta 68, 557–571. https://doi.org/10.1016/S0016-7037(03)00460-5

Karpoff, A.M., France-Lanord, C., Lothe, F., Karcher, P., 1992. Miocene Tuff from Mariana Basin, Leg 129, Site 802: A First Deep-Sea Occurrence of Thaumasite, in: Proceedings of the Ocean Drilling Program, 129 Scientific Results, Proceedings of the Ocean Drilling Program. Ocean Drilling Program. https://doi.org/10.2973/odp.proc.sr.129.113.1992

Keys, J.R., Williams, K., 1981. Origin of crystalline, cold desert salts in the McMurdo region, Antarctica. Geochimica et Cosmochimica Acta 45, 2299–2309. https://doi.org/10.1016/0016-7037(81)90084-3

Lehr, J.R., Frazier, A.W., Smith, J.P., 1964. A New Calcium Aluminum Phosphate, CaAlH(PO4)2·6H2O1. Soil Science Society of America Journal 28, 38–39. https://doi.org/10.2136/sssaj1964.03615995002800010024x

Mahaffy, P.R., Webster, C.R., Atreya, S.K., Franz, H., Wong, M., Conrad, P.G., Harpold, D., Jones, J.J., Leshin, L.A., Manning, H., Owen, T., Pepin, R.O., Squyres, S., Trainer, M., MSL Science Team, 2013. Abundance and Isotopic Composition of Gases in the Martian Atmosphere from the Curiosity Rover. Science 341, 263–266. https://doi.org/10.1126/science.1237966

Maher, B.A., Taylor, R.M., 1988. Formation of ultrafine-grained magnetite in soils. Nature 336, 368–370. https://doi.org/10.1038/336368a0

Matschei, T., Lothenbach, B., Glasser, F.P., 2007. Thermodynamic properties of Portland cement hydrates in the system CaO–Al2O3–SiO2–CaSO4–CaCO3–H2O. Cement and Concrete Research 37, 1379–1410. https://doi.org/10.1016/j.cemconres.2007.06.002

McAdam, A.C., Zolotov, M.Y., Mironenko, M.V., Sharp, T.G., 2008. Formation of silica by low-temperature acid alteration of Martian rocks: Physical-chemical constraints. Journal of Geophysical Research: Planets 113. https://doi.org/10.1029/2007JE003056

McCanta, M.C., Dyar, M.D., Treiman, A.H., 2014. Alteration of Hawaiian basalts under sulfur-rich conditions: Applications to understanding surface-atmosphere interactions on Mars and Venus†. American Mineralogist 99, 291–302. https://doi.org/10.2138/am.2014.4584

Meunier, A., 2005. Clays. Springer Science & Business Media.

Ming, D.W., Boettinger, J.L., 2001. Zeolites in Soil Environments. Reviews in Mineralogy and Geochemistry 45, 323–345. https://doi.org/10.2138/rmg.2001.45.11

Noack, Y., 1983. Occurrence of thaumasite in a seawater-basalt interaction, mururoa atoll (French Polynesia, South Pacific). Mineralogical Magazine 47, 47–50. https://doi.org/10.1180/minmag.1983.047.342.08

Oxmann, J.F., Schwendenmann, L., 2015. Authigenic apatite and octacalcium phosphate formation due to adsorption–precipitation switching across estuarine salinity gradients. Biogeosciences 12, 723–738. https://doi.org/10.5194/bg-12-723-2015

Oxmann, J.F., Schwendenmann, L., 2014. Quantification of octacalcium phosphate, authigenic apatite and detrital apatite in coastal sediments using differential dissolution and standard addition. Ocean Sci. 10, 571–585. https://doi.org/10.5194/os-10-571-2014

Pipilikaki, P., Papageorgiou, D., Teas, Ch., Chaniotakis, E., Katsioti, M., 2008. The effect of temperature on thaumasite formation. Cement and Concrete Composites 30, 964–969. https://doi.org/10.1016/j.cemconcomp.2008.09.004

Postma, D., 1982. Pyrite and siderite formation in brackish and freshwater swamp sediments. American Journal of Science 282, 1151–1183. https://doi.org/10.2475/ajs.282.8.1151

Postma, D., 1980. Formation of siderite and vivianite and the pore-water composition of a Recent bog sediment in Denmark. Chemical Geology 31, 225–244. https://doi.org/10.1016/0009-2541(80)90088-1

Rampe, E.B., Ming, D.W., Blake, D.F., Bristow, T.F., Chipera, S.J., Grotzinger, J.P., Morris, R.V., Morrison, S.M., Vaniman, D.T., Yen, A.S., Achilles, C.N., Craig, P.I., Des Marais, D.J., Downs, R.T., Farmer, J.D., Fendrich, K.V., Gellert, R., Hazen, R.M., Kah, L.C., Morookian, J.M., Peretyazhko, T.S., Sarrazin, P., Treiman, A.H., Berger, J.A., Eigenbrode, J., Fairén, A.G., Forni, O., Gupta, S., Hurowitz, J.A., Lanza, N.L., Schmidt, M.E., Siebach, K., Sutter, B., Thompson, L.M., 2017. Mineralogy of an ancient lacustrine mudstone succession from the Murray formation, Gale crater, Mars. Earth and Planetary Science Letters 471, 172–185. https://doi.org/10.1016/j.epsl.2017.04.021

Reed, M.H., 1998. Calculation of simultaneous chemical equilibria in aqueous-mineral-gas systems and its application to modeling hydrothermal processes, in: Richards, J.P. (Ed.), Techniques in Hydrothermal Ore Deposits Geology, Reviews in Economic Geology. Society of Economic Geologists, Inc., Littleton, CO, pp. 109–124.

Romanek, C.S., Jiménez-López, C., Navarro, A.R., Sánchez-Román, M., Sahai, N., Coleman, M., 2009. Inorganic synthesis of Fe–Ca–Mg carbonates at low temperature. Geochimica et Cosmochimica Acta 73, 5361–5376. https://doi.org/10.1016/j.gca.2009.05.065

Rosenqvist, I.Th., 1970. Formation of vivianite in holocene clay sediments. Lithos 3, 327–334. https://doi.org/10.1016/0024-4937(70)90039-3
Schmidt, T., Lothenbach, B., Romer, M., Scrivener, K., Rentsch, D., Figi, R., 2008. A thermodynamic and experimental study of the conditions of thaumasite formation. Cement and Concrete Research 38, 337–349. https://doi.org/10.1016/j.cemconres.2007.11.003
Schoonen, M.A.A., 2004. Mechanisms of sedimentary pyrite formation, in: Special Paper 379: Sulfur Biogeochemistry - Past and Present. Geological Society of America, pp. 117–134. https://doi.org/10.1130/0-8137-2379-5.117
Sharp, Z.D., Papike, J.J., Durakiewicz, T., 2003. The effect of thermal decarbonation on stable isotope compositions of carbonates. American Mineralogist 88, 87–92. https://doi.org/10.2138/am-2003-0111
Singer, A., Stahr, K., Zarei, M., 1998. Characteristics and origin of sepiolite (Meerschaum) from Central Somalia. Clay miner. 33, 349–362. https://doi.org/10.1180/000985598545525
Spiroff, K., 1938. Magnetite crystals from meteoric solutions. Economic Geology 33, 818–828. https://doi.org/10.2113/gsecongeo.33.8.818
Taylor, A.W., Gurney, E.L., 1965. Precipitation of Phosphate by Iron Oxide and Aluminum Hydroxide from Solutions Containing Calcium and Potassium1. Soil Science Society of America Journal 29, 18–22. https://doi.org/10.2136/sssaj1965.03615995002900010008x
Taylor, A.W., Gurney, E.L., 1964. The Dissolution of Calcium Aluminum Phosphate, CaAlH(PO4)2·6H2O1. Soil Science Society of America Journal 28, 63–64. https://doi.org/10.2136/sssaj1964.03615995002800010032x
Taylor, A.W., Gurney, E.L., Moreno, E.C., 1964. Precipitation of Phosphate from Calcium Phosphate Solutions by Iron Oxide and Aluminum Hydroxide1. Soil Science Society of America Journal 28, 49–52. https://doi.org/10.2136/sssaj1964.03615995002800010028x
Taylor, R.M., Maher, B.A., Self, P.G., 1986. Magnetite in soils: I. The synthesis of single-domain and superparamagnetic magnetite. Clay Minerals 22, 411–422. https://doi.org/10.1180/claymin.1987.022.4.05
Tosca, N.J., Guggenheim, S., Pufahl, P.K., 2016. An authigenic origin for Precambrian greenalite: Implications for iron formation and the chemistry of ancient seawater. GSA Bulletin 128, 511–530. https://doi.org/10.1130/B31339.1
Vaniman, D.T., Bish, D.L., Ming, D.W., Bristow, T.F., Morris, R.V., Blake, D.F., Chipera, S.J., Morrison, S.M., Treiman, A.H., Rampe, E.B., Rice, M., Achilles, C.N., Grotzinger, J.P., McLennan, S.M., Williams, J., Bell, J.F., Newsom, H.E., Downs, R.T., Maurice, S., Sarrazin, P., Yen, A.S., Morookian, J.M., Farmer, J.D., Stack, K., Milliken, R.E., Ehlmann, B.L., Sumner, D.Y., Berger, G., Crisp, J.A., Hurowitz, J.A., Anderson, R., Des Marais, D.J., Stolper, E.M., Edgett, K.S., Gupta, S., Spanovich, N., MSL Science Team, 2014. Mineralogy of a Mudstone at Yellowknife Bay, Gale Crater, Mars. Science 343. https://doi.org/10.1126/science.1243480
Vayssières, L., Chanéac, C., Tronc, E., Jolivet, J.P., 1998. Size Tailoring of Magnetite Particles Formed by Aqueous Precipitation: An Example of Thermodynamic Stability of Nanometric Oxide Particles. Journal of Colloid and Interface Science 205, 205–212. https://doi.org/10.1006/jcis.1998.5614
Warren, J.K., 2015. Evaporites: a geological compendium. Springer Berlin Heidelberg, New York, NY.
Wilson, M.D., Pittman, E.D., 1977. Authigenic clays in sandstones: recognition and influence on reservoir properties and paleoenvironmental analysis. Journal of Sedimentary Research 47.